# Two-stage linear-nonlinear shaping of an optical frequency comb as rogue nonlinear-Schrödinger-equation-solution generator

Benoit Frisquet, Amin Chabchoub, Julien Fatome, Christophe Finot, Bertrand Kibler, Guy Millot

# Two-stage linear-nonlinear shaping of an optical frequency comb as rogue nonlinear-Schrödinger-equation-solution generator

B. Frisquet,[1] A. Chabchoub,[2,1] J. Fatome,[1] C. Finot,[1] B. Kibler,[1,*] and G. Millot[1]

[1]*Laboratoire Interdisciplinaire Carnot de Bourgogne (ICB), UMR 6303 CNRS–Université de Bourgogne, 21078 Dijon, France*

[2]*Centre for Ocean Engineering Science and Technology, Swinburne University of Technology, Hawthorn, Victoria 3122, Australia*

(Received 15 November 2013; published 14 February 2014)

We report a wave generator of complex solutions of the nonlinear Schrödinger equation (NLSE) combining both intensity and phase spectral shaping of an initial optical frequency comb with subsequent nonlinear propagation in an optical fiber. We apply the explicit analytical form of the two-breather solutions of the NLSE as a linear spectral filter to shape ideal modulation of a continuous wave. The additional nonlinear propagation of the tailored wave provides experimental evidence of both the growth and decay of the fundamental second-order periodic breather solution. The temporal and spectral profiles of the higher-order breather are in excellent agreement with the corresponding analytical solution.

DOI: 10.1103/PhysRevA.89.023821 PACS number(s): 42.65.Tg, 05.45.−a

Complex periodic solutions of the nonlinear Schrödinger equation (NLSE), known as solitons on a finite background or breathers, have attracted particular attention during recent years since they are considered as prototypes to model extreme energy localization in many nonlinear dispersive systems [1,2]. These localized waves are observed when small-amplitude perturbations on a continuous wave (cw) become strongly focused due to modulation instability of nonlinear waves, thus providing a simple approach for the description of the famous hydrodynamic rogue wave formation [3–6]. Their existence has also been confirmed in other fields of physics driven by the NLSE [7–9]. The first experimental studies on breathers have already demonstrated that nonideal initial perturbations may lead to the generation of complex behaviors that may differ from the expected mathematical solution of single breathers [10,11]. In particular, the sensitivity to initial perturbations depends on the complexity or order of the solution (i.e., the order of energy localization). In water wave experiments, the initial wave profiles are generated with a paddle located at one end of a tank. An electric signal, derived from the exact mathematical expression describing the water surface elevation, drives the paddle to directly modulate the surface height. Specific initial modulations such as a ratio of polynomials have been applied to the wave maker to excite super-rogue waves [5,12,13]. However, such ideal perturbations in optics are nontrivial to synthesize in the temporal domain by means of the usual intensity modulators at gigahertz levels. Previous experiments in optics have used only sinusoidal modulations [8,10].

In this context we propose to introduce the advantages of ultrafast optics technology and programmable optical pulse shaping that allow the generation of nearly arbitrarily shaped ultrafast optical wave forms [14,15]. Shaped laser pulses have already demonstrated their potential for many applications such as telecommunications systems, multiphoton microscopy, and coherent control of quantum systems. Here we consider Fourier-transform optical pulse shaping in order to provide the ultimate control in terms of phase and amplitude for achieving the ideal excitation of complex NLSE solutions. In particular, our optical processing is based on spectral line-by-line shaping of a frequency comb generator [16], which is well suited for studies of time-periodic NLSE solutions. Nonlinear wave propagation is next completed in a standard optical fiber to analyze both temporal and spectral evolutions compared to mathematical predictions. In this paper, we describe the experimental observation of both the growth and decay of the fundamental second-order periodic breather solution by exploiting the two-stage linear-nonlinear shaping of an optical frequency comb at telecommunications wavelengths. This work opens the way to experimental investigations of the rich family of complex solutions of the NLSE by using low-cost optical-fiber-based systems and may motivate similar experiments in other nonlinear dispersive media, governed by the NLSE.

The self-focusing NLSE is written in dimensionless form as $i\psi_\xi + (1/2)\psi_{\tau\tau} + \psi^2\psi = 0$, where subscripted variables stand for partial differentiations. $\psi$ is a wave group or pulse envelope which is a function of $\xi$ (a propagation distance or longitudinal variable) and $\tau$ (a comoving time or transverse variable). General first-order breather solutions of the NLSE are usually associated with the following explicit wording: solitons on a finite background [8,17]. These fundamental solutions are either periodic in space and localized in time or periodic in time and localized in space; they are referred to as Kuznetsov-Ma solitons (KMSs) and Akhmediev breathers (ABs), respectively. Taking the period of both solutions to infinity gives rise to a first-order doubly localized Peregrine soliton (PS). Here we are interested in fundamental two-breather solutions (i.e., second-order NLSE solutions) that correspond to the nonlinear superposition of two first-order elementary breathers [18]. The dynamics of such solutions describes the interaction in the plane $(\xi,\tau)$ between fundamental ABs, KMSs, and PSs. Various forms of the second-order periodic solutions have been recently derived [18]. Nonlinear superposition of several breathers has already been observed in optics by stimulating the modulation instability process with a single or a combination of two cosine modulations [11,19,20], but the generated breathers only approach the exact solutions. Up to date, only one case of a second-order NLSE solution has been experimentally studied with exact initial conditions [12,13]; it concerns the

*Corresponding author: bertrand.kibler@u-bourgogne.fr

 

limiting rational case of synchronized superposition of PSs. The experiments related to this solution were performed for water waves by splitting its evolution into several stages of propagation and by reconstructing the wave dynamics afterwards in order to overcome the restriction in terms of wave flume length [12]. More precisely, after starting the breather wave generation repetitively with different boundary conditions provided from theory, the measured wave profiles, collected at the other end of the tank, were then compared to the corresponding theoretical predictions. Deviations from theory were minimal so that this process was repeated several times to reach a long propagation distance, which corresponds to the point of maximum wave amplitude. We propose to apply this technique to our nonlinear propagation stage to overcome here the impact of fiber losses on the full evolution of the wave profiles related to the higher-order breather solutions.

The first stage of our setup is based on spectral line-by-line shaping of an optical frequency comb, which synthesizes time-periodic initial perturbations. Consequently, it restricts our present study to nonlinear superposition of several ABs with commensurate frequencies. In the following, we illustrate our work by generating a synchronized nonlinear superposition of two ABs with two different modulation frequencies; in particular with a frequency ratio of 2:1. Each first-order breather $j$ in the higher-order solution is described by the governing parameter $a_j$, the modulation frequency $\omega_j = 2(1-2a_j)^{1/2}$, the instability growth rate $b_j = [8a_j(1-2a_j)]^{1/2}$, and a shifted point of origin $(\xi_j,\tau_j)$ [7,10,18]. The second-order breather solution is given in Ref. [18] as

$$\psi_2(\xi,\tau) = e^{i\xi}\left[1+\frac{G_2+iH_2}{D_2}\right],$$

$$G_2 = -\left(\omega_1^2-\omega_2^2\right)\left[\frac{\omega_1^2 b_2}{\omega_2}\cosh(b_1\xi_{s1})\cos(\omega_2\tau_{s2}) - \frac{\omega_2^2 b_1}{\omega_1}\cosh(b_2\xi_{s2})\cos(\omega_1\tau_{s1}) - \left(\omega_1^2-\omega_2^2\right)\cosh(b_1\xi_{s1})\cosh(b_2\xi_{s2})\right],$$

$$H_2 = -2\left(\omega_1^2-\omega_2^2\right)\left[\frac{b_1 b_2}{\omega_2}\sinh(b_1\xi_{s1})\cos(\omega_2\tau_{s2}) - \frac{b_1 b_2}{\omega_1}\sinh(b_2\xi_{s2})\cos(\omega_1\tau_{s1})\right.$$
$$\left. - \mathrm{b}_1\sinh(b_1\xi_{s1})\cosh(b_2\xi_{s2}) + \mathrm{b}_2\sinh(b_2\xi_{s2})\cosh(b_1\xi_{s1})\right], \quad (1)$$

$$D_2 = 2\left(\omega_1^2+\omega_2^2\right)\frac{b_1 b_2}{\omega_1\omega_2}\cos(\omega_1\tau_{s1})\cos(\omega_2\tau_{s2}) + 4b_1 b_2[\sin(\omega_1\tau_{s1})\sin(\omega_2\tau_{s2})$$
$$+ \sinh(b_1\xi_{s1})\sinh(b_2\xi_{s2})] - \left(2\omega_1^2 - \omega_1^2\omega_2^2 + 2\omega_2^2\right)\cosh(b_1\xi_{s1})\cosh(b_2\xi_{s2})$$
$$- 2\left(\omega_1^2-\omega_2^2\right)\left[\frac{b_1}{\omega_1}\cos(\omega_1\tau_{s1})\cosh(b_2\xi_{s2}) - \frac{b_2}{\omega_2}\cos(\omega_2\tau_{s2})\cosh(b_1\xi_{s1})\right],$$

where $\xi_{sj} = \xi - \xi_j$ and $\tau_{sj} = \tau - \tau_j$ are shifted variables. In this study, we consider a synchronized nonlinear superposition at the origin so that $\xi_1 = \xi_2 = 0$ and $\tau_1 = \tau_2 = 0$. The above solution describes the full wave evolution of the second-order breather during its nonlinear propagation.

The experimental setup depicted in Fig. 1 is based on high-speed telecommunications-grade components. It benefits from a different fiber-based test bed in comparison to previous studies of single breathers in optics [7,8]. The initial frequency comb is generated by the implementation of a 20-GHz repetition rate pulse source centered at 1550 nm based on the nonlinear compression of an initial beatsignal in a cavityless optical-fiber-based device. To generate the initial beat signal we used an external cavity laser (ECL) diode combined with a $LiNbO_3$ intensity modulator (IM) driven by a 20-GHz external rf clock. A phase modulator (PM), driven at 100 MHz, is also introduced to prevent the detrimental effect of stimulated Brillouin backscattering in our experiment. The resulting sinusoidal beat signal is amplified to an optimal average power (here 0.45 W) by means of an erbium-doped fiber amplifier (EDFA) before injection into the compression fiber. The nonlinear compression takes place in a 2.1-km-long segment of standard single-mode fiber (SMF1) with group velocity dispersion $\beta_2 = -20.4\ \mathrm{ps}^2\ \mathrm{km}^{-1}$, linear losses $\alpha_{\mathrm{dB}} = 0.3\ \mathrm{dB\ km}^{-1}$, and nonlinearity $\gamma = 1.2\ \mathrm{W}^{-1}\ \mathrm{km}^{-1}$.More details about similar fiber-based frequency combs can be found in Refs. [21,22]. Measurements of both temporal and spectral profiles of the frequency comb are reported in Figs. 1(b) and 1(c). The spectrum of such a pulse source can be approximated as a series of Dirac $\delta$functions separated by the repetition rate. The width of the comb envelope depends on the nonlinear compression of the initial modulated cw and it determines the number of sidebands and their decreasing amplitude. The input average power was determined according to the modulation amplitude of the initial beat signal to optimize the output spectral bandwidth without significant pump depletion, thus leading to the typical triangular spectrum on a logarithmic scale well suited for studies of breathers [23,24].

Next a programmable optical filter (wave shaper) provides an extremely fine control of the amplitude and phase characteristics of each line of the frequency comb. The high resolution ($\sim$1 GHz) of this solid-state liquid crystal on silicon system allows us to select or control individual spectral peaks of the comb [25]. Relative amplitude and phase differences

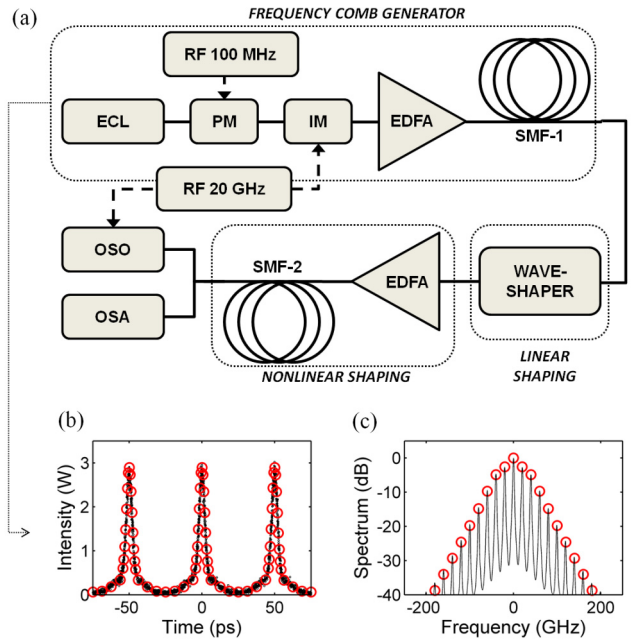


FIG. 1. (Color online) (a) Experimental setup. ECL, external cavity laser diode; PM, phase modulator; IM, intensity modulator; EDFA, erbium-doped fiber amplifier; SMF, single-mode fiber; OSA, optical spectrum analyzer; OSO, optical sampling oscilloscope. Experimental profiles (black lines) of the frequency comb generator in both time (b) and frequency (c) domains measured with the help of the OSO and OSA, respectively. Corresponding numerical simulations (red circles) based on the NLSE including fiber losses.

of 24 sidebands with the central peak at 1550 nm (i.e., the background wave) are managed to define the exact initial conditions to stimulate the second-order periodic breather solution in the fiber. An EDFA is used to amplify the average power of the synthesized wave before coupling into another 1.5-km-long segment of standard optical fiber (SMF2) with group velocity dispersion $\beta_2 = -21.1\ \mathrm{ps}^2\,\mathrm{km}^{-1}$, linear losses $\alpha_{\mathrm{dB}} = 0.3\ \mathrm{dB\,km}^{-1}$, and nonlinearity $\gamma = 1.2\ \mathrm{W}^{-1}\,\mathrm{km}^{-1}$. The average power of the input wave is fixed so that it satisfies the values of the general parameters $a_j$ using the fiber properties (see below for rescaling in dimensional units). At the fiber output, the optical wave profile is characterized using an ultrafast optical sampling oscilloscope (OSO) with subpicosecond resolution and a high-dynamic-range optical spectrum analyzer (OSA) with 2.5 GHz resolution.

To illustrate the principle of operation of the complex nonlinear wave generator, we have performed numerical simulations based on the NLSE using the initial characterization of the frequency comb. In Fig. 2, we show the particular case for which we obtain the maximal amplitude of the second-order solution at the fiber output. For this the initial condition at the fiber input has to be equal to $\psi_{\mathrm{IN}} = \psi_2(\xi = -L_{\mathrm{SMF2}}/L_{\mathrm{NL}}, \tau)$, with the fiber length $L_{\mathrm{SMF2}} = 1.5$ km. This requires only a calculation of spectral (phase and intensity) profile differences between the initial frequency comb and the corresponding Fourier transform $\tilde{\psi}_{\mathrm{IN}}$; next one can apply the resulting (phase and intensity) corrections as a pulse shaping mask to the wave shaper.

The correspondence between theory and experiment can be retrieved by recalling that dimensional distance $z$ (m) and time $t$ (s) are related to the previous normalized parameters by $z = \xi L_{\mathrm{NL}}$ and $t = \tau t_0$, where the characteristic (nonlinear) length and time scales are $L_{\mathrm{NL}} = (\gamma P_0)^{-1}$ and $t_0 = (|\beta_2| L_{\mathrm{NL}})^{1/2}$, respectively. The dimensional field $A(z,t)$ $(\mathrm{W}^{1/2})$ is $A = P_0^{1/2}\psi$, $P_0$ being the average power of the input wave. The modulation frequency $\omega_{\mathrm{mod}}$ of a single breather is related to the general governing parameter $a$ by $2a = [1 - (\omega_{\mathrm{mod}}/\omega_c)^2]$, where the critical frequency value of the modulation instability gain is given by $\omega_c^2 = 4\gamma P_0/\beta_2$ [10]. For simulation and experiment, the parameters used are the following: $P_0 = 0.513$ W, $\beta_2$ and $\gamma$ are fiber parameters from the SMF2, $a_1 = 0.2294$ ($\omega_{\mathrm{mod1}} = 40$ GHz), and $a_2 = 0.4323$ ($\omega_{\mathrm{mod2}} = 20$ GHz).

Figure 2 shows three stages of the evolution of temporal intensity, spectral phase, and spectral intensity which correspond to (a) the initial frequency comb, (b) the synthesized input wave, and (c) the fiber output wave. The numerical results are compared to the analytic solution of the

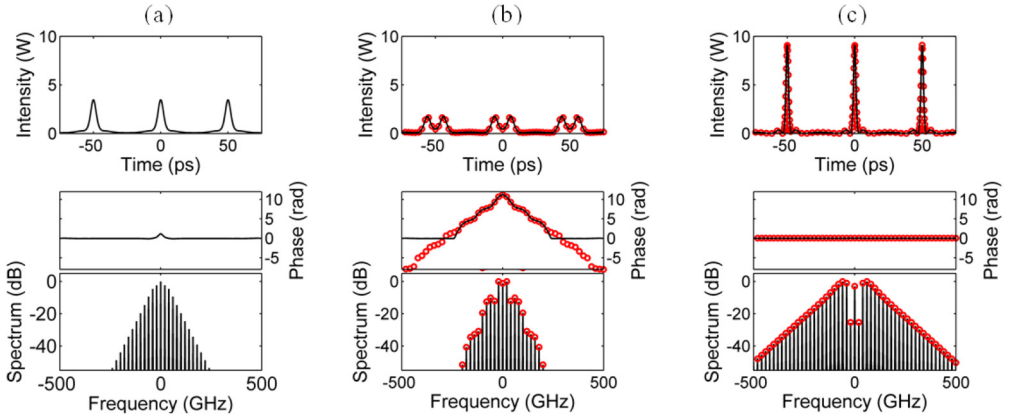


FIG. 2. (Color online) Evolution of temporal intensity, (unwrapped) spectral phase, and spectral intensity in our second order breather generator which correspond to (a) the initial frequency comb, (b) the synthesized input wave using a linear shaping, and (c) the fiber output wave resulting from the nonlinear shaping. Solid black lines and red circles correspond to NLSE simulations and the theoretical solution given by Eq. (1), respectively.

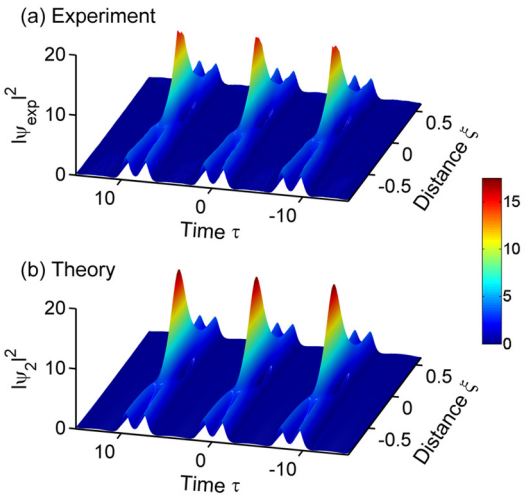


FIG. 3. (Color online) Evolution of the second-order periodic breather in the temporal domain as a function of propagation distance. (a) Experiments. (b) Analytic solution given by Eq. (1). Note that dimensional distance and time are normalized here for better comparison with theory.

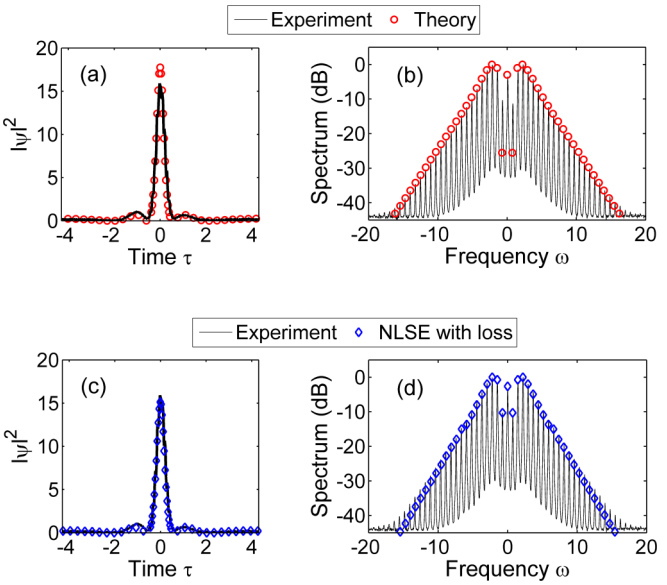


FIG. 4. (Color online) Comparison between experiment (black lines) and theory (red circles) at the distance corresponding to the maximal amplitude of the second-order solution. (a) Temporal intensity profile. (b) Corresponding spectral profile. (c) and (d) Similar comparison between experiment (black lines) and NLSE simulation taking into account linear fiber losses (blue diamonds). Note also that both experimental and simulated intensity profiles are normalized to the input average power $P_0$.

second-order solution given by Eq. (1) for the last two stages: (b) $\psi_2(\xi = -L_{\mathrm{SMF2}}/L_{\mathrm{NL}},\tau)$ and (c) $\psi_2(\xi = 0,\tau)$, respectively. The excellent agreement between the simulation results and the theoretical solution is confirmed, but this requires a careful (phase and amplitude) shaping of each line of the frequency comb. Note that the spectral phase of the initial frequency comb is obtained from numerical simulations corresponding to our frequency comb generator described above. The agreement between experimental measurements and simulations shown in Figs. 1(b) and 1(c) ensures a good estimate of the spectral phase used in Fig. 2(a).

In order to validate our complex NLSE solution generator, we have experimentally investigated the parameters of nonlinear superposition described above. Inspired by a hydrodynamic higher-order breather experiment, we have also applied an original method for reconstructing the wave evolution as a function of propagation distance, benefiting from the programmable wave shaper. Indeed, the initial shaped conditions for the nonlinear propagation are generated repetitively with different boundary conditions, given from theory, in order to reach a long propagation distance (without additional fiber losses). In fact, we consider only short nonlinear propagation sequences in the SMF2 of about $0.92L_{\mathrm{NL}}$. First, we begin with initial conditions fixed at a position 3 km from the maximal breather amplitude and in the next step we record at the fiber output. Subsequently, we proceed with a propagation step equal to 0.1 km ($0.0616L_{\mathrm{NL}}$) to generate new initial conditions from the theory. Repetition of this recording process 25 times allows the accurate observation of the nonlinear wave evolution over 2.5 km, which corresponds to the value $1.54L_{\mathrm{NL}}$, as shown in Fig. 3. Additional propagation could be investigated by using other adjustments of the initial frequency comb characteristics (power, bandwidth). As shown in Fig. 3(a), we clearly observe both growth and decay of the second-order periodic breather. Specific characteristics are revealed, such as the time-periodic central second-order wave peak due to the merging of the two AB components, but also the typical X-shape signature in the plane $(\xi,\tau)$. One can note that the high-amplitude central peak appears and disappears over less than half of the nonlinear length. The experimental results are compared to the analytic solution given by Eq. (1) in Fig. 3(b). Note also that the experimental intensity profile is normalized to the input average power $P_0$. The agreement is remarkable for the entire evolution measured in the plane $(\xi,\tau)$.

Figure 4 gives an explicit comparison at a distance corresponding to the maximal amplitude of the second-order solution. Only small discrepancies with theory appear for the peak intensity. We underline that only the fiber losses, which are equal to 0.3 dB km$^{-1}$, affect the results obtained. Indeed, the experimental wave profile in the time and frequency domains is indistinguishable from predictions given by NLSE simulations taking into account the linear losses [see Figs. 4(c) and 4(d)]. The resulting misfit parameter between the experimental shape and theory, defined as $M = \int(\overline{|\psi_{\mathrm{expt}}|^2} - \overline{|\psi_2|^2})^2 dt / \int(\overline{|\psi_{\mathrm{expt}}|^2})^2\, dt$, is below 4% [here, $\overline{|\psi_j|^2}$ denotes the normalized shape, i.e., $\max(\overline{|\psi_j|^2}) = 1$].

To complete our experimental characterization, spectral measurements have also been performed [see Fig. 4(b)]. Multiple sideband generation is clearly observed when compared to the initial spectrum of the frequency comb shown in Fig. 1(c). In particular, we have checked that the inverse Fourier transform of the experimental spectrum is close to the temporal profile measured, thus indicating that the generated pulses exhibit a near-flat spectral phase as expected from Fig. 2(c). The excellent signal-to-noise ratio in our experiments allows the theoretical predictions to be satisfied over a 40 dB dynamic

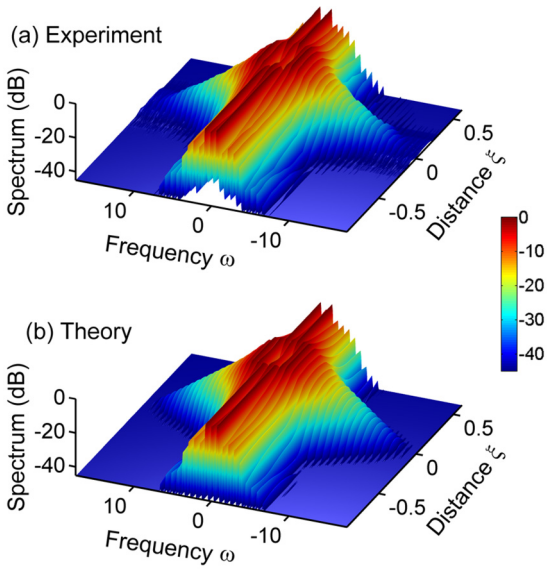


FIG. 5. (Color online) Evolution of the second-order breather in the frequency domain as a function of propagation distance. (a) Experiments. (b) Analytic solution given by Eq. (1). Note that dimensional distance and frequency are normalized here for a better comparison with theory.

range. Note also that the main frequency modulation of the breather spectrum is $\omega_2$ ($\omega_{\mathrm{mod2}}$ =20 GHz), which corresponds to the temporal period of the central second-order wave peak. The full experimental evolution of the higher-order breather in the frequency domain is shown in Fig. 5(a). A strong spectral broadening occurs when the second-order breather reaches its maxima of temporal compression and peak intensity. As in previous studies of single breathers, we confirm that the temporal compression is associated with an increased spatial localization of the energy transfer to higher sideband orders along the propagation distance (this energy transfer occurs in less than $0.5L_{\mathrm{NL}}$ in Fig. 5). The agreement between the spectral evolution recorded and the theoretical solution is again excellent [see Fig. 5(b)].

In conclusion, we have experimentally confirmed that complex periodic solutions of the NLSE can be generated in nonlinear fiber optics by using exact initial modulated waves. The synthesized input conditions rely on a spectral line-by-line shaping of an optical frequency comb. Moreover we have used the original approach of short propagation sequences for reconstructing the full wave evolution, thus allowing the observation of both the growth and decay of an ideal second-order breather. This technique overcomes the destructive cutback method required for direct measurements of the longitudinal evolution. Experimental measurements of the synchronized nonlinear superposition of two Akhmediev breathers are in excellent agreement with the theoretical solution. The experimental proof of both the existence and control of such complex waves is of fundamental importance for testing theories of nonlinear wave dynamics in cross-disciplinary research.

We acknowledge support from the French National Research Agency (Grants No. ANR-12-BS04-0011OPTIROC and No. ANR-11-EMMA-0005 SOFAST), from the Conseil Régional de Bourgogne through a Photcom PARI grant, and from the iXCore Foundation. A.C. acknowledges support from ARC Discovery Grants No. DP1093349 and No. DP1093517. This work has been performed in cooperation with the Labex ACTION program (Contract No. ANR-11-LABX-01-01).

[1] N. Akhmediev, J. M. Soto-Crespo, and A. Ankiewicz, Phys. Lett. A **373**, 2137 (2009).
[2] M. Onorato, S. Residori, U. Bortolozzo, A. Montina, and F. T. Arecchi, Phys. Rep. **528**, 47 (2013).
[3] C. Kharif, E. Pelinovsky, and A. Slunyaev, *Rogue Waves in the Ocean* (Springer-Verlag, Berlin, 2009).
[4] A. R. Osborne, *Nonlinear Ocean Waves and the Inverse Scattering Transform* (Academic Press, San Diego, 2010).
[5] A. Chabchoub, N. P. Hoffmann, and N. Akhmediev, Phys. Rev. Lett. **106**, 204502 (2011).
[6] M. Onorato, D. Proment, G. Clauss, and M. Klein, PLoS One **8**, e54629 (2013).
[7] B. Kibler, J. Fatome, C. Finot, G. Millot, F. Dias, G. Genty, N. Akhmediev, and J. M. Dudley, Nat. Phys. **6**, 790 (2010).
[8] B. Kibler, J. Fatome, C. Finot, G. Millot, G. Genty, B. Wetzel, N. Akhmediev, F. Dias, and J. M. Dudley, Sci. Rep. **2**, 463 (2012).
[9] H. Bailung, S. K. Sharma, and Y. Nakamura, Phys. Rev. Lett. **107**, 255005 (2011).
[10] J. M. Dudley, G. Genty, F. Dias, B. Kibler, and N. Akhmediev, Opt. Express **17**, 21497 (2009).
[11] K. Hammani, B. Kibler, C. Finot, P. Morin, J. Fatome, J. M. Dudley, and G. Millot, Opt. Lett. **36**, 112 (2011).
[12] A. Chabchoub, N. P. Hoffmann, M. Onorato, and N. Akhmediev, Phys. Rev. X **2**, 011015 (2012).
[13] A. Chabchoub, N. Hoffmann, M. Onorato, A. Slunyaev, A. Sergeeva, E. Pelinovsky, and N. Akhmediev, Phys. Rev. E **86**, 056601 (2012).
[14] S. T. Cundiff and A. M. Weiner, Nat. Photonics **4**, 760 (2010).
[15] A. M. Weiner, Opt. Commun. **284**, 3669 (2011).
[16] Z. Jiang, D. E. Leaird, C-B. Huang, H. Miao, M. Kourogi, K. Imai, and A. M. Weiner, IEEE J. Quantum Electron. **43**, 1163 (2007).
[17] N. Akhmediev, V. M. Eleonskii, and N. E. Kulagin, J. Exp. Theor. Phys. **62**, 894 (1985).
[18] D. J. Kedziora, A. Ankiewicz, and N. Akhmediev, Phys. Rev. E **85**, 066601 (2012).
[19] M. Erkintalo, K. Hammani, B. Kibler, C. Finot, N. Akhmediev, J. M. Dudley, and G. Genty, Phys. Rev. Lett. **107**, 253901 (2011).
[20] B. Frisquet, B. Kibler, and G. Millot, Phys. Rev. X **3**, 041032 (2013).
[21] C. Fortier, B. Kibler, J. Fatome, C. Finot, S. Pitois, and G. Millot, Laser Phys. Lett. **5**, 817 (2008).

[22] I. El Mansouri, J. Fatome, C. Finot, M. Lintz, and S. Pitois, IEEE Photon. Technol. Lett. **23**, 1487 (2011).

[23] N. Akhmediev, A. Ankiewicz, J. M. Soto-Crespo, and J. M. Dudley, Phys. Lett. A **375**, 775 (2011).

[24] K. Hammani, B. Wetzel, B. Kibler, J. Fatome, C. Finot, G. Millot, N. Akhmediev, and J. M. Dudley, Opt. Lett. **36**, 2140 (2011).

[25] A. M. Clarke, D. G. Williams, M. A. F. Roelens, and B. J. Eggleton, J. Lightwave Technol. **28**, 97 (2010).